

Transient Coupled Thermoelastic Contact Problems Incorporating Thermal Resistance: a BEM Approach

L.K. Keppas¹, G.I. Giannopoulos¹ and N.K. Anifantis¹

Abstract: In the present paper a boundary element procedure is formulated to treat two-dimensional time dependent thermo-elastic contact problems incorporating thermal resistance along the contacting surfaces. The existence of pressure-dependent thermal contact leads to coupling of temperature and stress fields. Therefore, the inherent non-linearity of the problem demands simultaneous treating of both thermal and mechanical boundary integral equations while iterative procedures are introduced to ensure equilibrium of mechanical and thermal contact conditions at each step of the process. The transient behavior of interfacial cracks in bimaterial solids when undergo thermal shock in the presence of partial crack closure and thermal contact resistance may be an interesting aspect of engineering design. For this purpose the methodology is applied on a thermal barrier coating system (TBC). Near crack tip singularities of temperature and displacement fields are modeled through appropriate quarter-point singular elements. Fracture parameters are evaluated from nodal tractions of singular elements utilizing proper formulas. Numerical results are compared with available solutions from the literature, where possible. Good agreement between them can be found.

Keyword: Thermal shock; coupled analysis; BEM; Thermal contact resistance; Interfacial crack; thermal barrier coating.

1 Introduction

In many technological problems the heat exchange between two bodies in contact may be

of high interest. The presence of imperfect contact and thermal resistance, which depends on the pressure between the contacting faces, leads to coupling of the thermal and stress field in such problems. Several studies dealing with heat transfer and thermoelastic problems take into account the imperfect contact and thermal resistance [Barber and Comninou (1983); Comninou and Barber (1984); Blandford and Tauchert (1985); Sih and Chen (1986); Kuo (1990); Zavarise, Wriggers, Stein and Schrefler (1992); Alonso and Garrido (1995); Alonso, Garrido, and Foces (1995); Kishimoto, Inoue and Shibuya (1995); Pantuso, Bathe and Bouzinov (2000); Martynyak, Honchar and Nahalka (2003); Hattiangadi and Siegmund (2005); Giannopoulos and Anifantis (2007)]. Among them there are analytical and numerical studies assuming time dependent or steady state thermoelasticity. A variety of thermoelastic problems has also been treated by several researchers employing advanced numerical methods [Chen and Liu (2001); Shiah, Guao and Tan (2005); Ching and Chen (2006); Sladek, Sladek, Zhang and Tan (2006)].

However, only a part of all the aforementioned studies considers the thermal resistance independent of the contact pressure. Additionally, over the last two decades there are not many published works about procedures capable of solving thermoelastic fracture problems of cracks which have their faces in full or partial contact incorporating in analysis the thermal contact resistance [Barber and Comninou (1983); Comninou and Barber (1984); Sih and Chen (1986); Kuo (1990); Shiah and Tan (2000); Martynyak, Honchar and Nahalka (2003); Hattiangadi and Siegmund (2005); Giannopoulos and Anifantis (2007)].

Interfacial cracks between solids with mismatch

¹Machine Design Laboratory, Mechanical and Aeronautics Engineering Department, University of Patras, Rion 26500, Greece.

in material properties, under environmental thermal changes have attracted considerable attention in the design of various composite structures. Special mechanical and thermal contact conditions must be employed in order to simulate realistically the contact phenomena and to evaluate the fracture parameters. The transient behavior of thermally stressed interfacial cracks, existing between dissimilar media, was examined by Kokini and Reynolds (1991). However, there is a lack of published works based on numerical methods in which the applied thermal conditions result in the closure of the crack. Few are as well, the analytical solutions given in the literature [Barber and Comninou (1983); Comninou and Barber (1984); Rizk Abd El-Fattah (1993); Martynyak, Honchar and Nahalka (2003)] involving crack closure phenomena caused by thermal loading. Since the non-linearities and the imposed contact conditions are located at the boundaries, the boundary element method (BEM) is a suitable technique for the analysis of this class of problems [Martinez and Dominguez (1984); Raveendra and Banerjee (1992); Alonso and Garrido (1995); Alonso, Garrido, and Foces (1995); Katsareas and Anifantis (1995); Kishimoto, Inoue and Shibuya (1995); Giannopoulos and Anifantis (2007)].

The demand for durable materials that can undergo extreme thermal environmental conditions turned the researcher's interest to thermal barrier coatings (TBCs), [Kokini and Reynolds (1991); Rangaraj and Kokini (2003); Arai, Okajima and Kishimoto (2007)] which provide thermal protection to the metallic substrates. However, these coatings have integrity problems, due to the material properties mismatches between the coating and the substrate and interfacial cracks can initiate in the presence of the developed stress field.

In the present study a BEM formulation, implemented in a home made computer code, is proposed for the solution of transient coupled problems of thermo-elasticity by assuming contact pressure-dependent thermal contact resistance (TCR) between contacting areas of dissimilar media. The formulation is based on the boundary integral equations for 2D time-dependent thermo-elasticity. A general contact problem of

two solids with different material properties is firstly investigated to verify the applicability of the formulation. Afterwards, the proposed BEM procedure is utilized in order to characterize thermomechanical fracture at the interface of thermal barrier coatings (TBC) under thermal shock. In this step, the impact of TCR of the partiality closed crack faces on the fracture severity is examined for such systems. Extensive parametric and sensitivity analyses in regard to the level of mismatch in material properties and several cases of friction coefficient and heat convection are examined assuming different scenarios of TCR. In essence the application of the proposed technique on TBC, yields valuable information for the design and fracture assessment of such systems. The singularities around the crack tip are approached using quarter-point elements (QPEs) [Martinez and Dominguez (1984); Katsareas and Anifantis (1995)]. Appropriate solutions from the literature are used, where possible, in order to validate the methodology and results.

2 Coupled boundary element analysis considering thermal contact resistance

2.1 Application of BEM to quasi-static thermo-elasticity

In the case of a two-dimensional solid defined on domain Ω of boundary Γ , the time dependent thermo-elastic behavior, in the absence of internal heat sources, is described by the following boundary integral equations [Brebbia, Telles and Wrobel (1984); Raveendra and Banerjee (1992)]:

$$\begin{aligned}
 c(\xi)\theta(\xi, t^F) + \int_{t^0}^{t^F} \int_{\Gamma} \theta(x, t) Q(x, \xi, t^F, t) d\Gamma(x) dt \\
 - \int_{\Omega} \theta^0(x) Q(x, \xi, t^F, t^0) d\Omega(x) \\
 = \int_{t^0}^{t^F} \int_{\Gamma} q(x, t) \Theta(x, \xi, t^F, t) d\Gamma(x) dt \quad (1)
 \end{aligned}$$

$$\begin{aligned}
 & c_{ij}(\xi)u_j(\xi, t^F) + \int_{\Gamma} u_j(x, t^F)T_{ij}(x, \xi)d\Gamma(x) \\
 &= \int_{\Gamma} t_j(x, t^F)U_{ij}(x, \xi)d\Gamma(x) \\
 &+ \int_{t^0}^{t^F} \int_{\Gamma} \left[\theta(x, t)\overline{Q}_i(x, \xi, t^F, t) \right. \\
 &\quad \left. - q(x, t)\overline{\Theta}_i(x, \xi, t^F, t) \right] d\Gamma(x)dt \quad (2)
 \end{aligned}$$

where i and j correspond to directions x_i and x_j , respectively, with $i, j = 1, 2$, x and ξ are points on the boundary Γ , c and c_{ij} are constants depending on the geometry at point ξ , θ and q denote temperature and heat flux, u_j and t_j denote components of the boundary displacement vector and traction vector, respectively, t is the time at which the responses are calculated, t^0 and t^F are the initial and final time points and θ^0 is the initial temperature. The functions $\Theta(x, \xi, t^F, t)$, $Q(x, \xi, t^F, t)$, $T_{ij}(x, \xi)$, $U_{ij}(x, \xi)$, $\overline{\Theta}_i(x, \xi, t^F, t)$, $\overline{Q}_i(x, \xi, t^F, t)$ represent the fundamental solutions for two-dimensional time-dependent thermo-elasticity available in the literature [Brebbia, Telles and Wrobel (1984)]. The boundary of the body is discretized into a number of standard 3-node quadratic isoparametric elements. Over each element the variations of the geometry, displacements and tractions are described in terms of nodal values, by the corresponding shape functions [Brebbia, Telles and Wrobel (1984)]. It is mentioned that standard quadratic elements are used everywhere in the boundary except for the crack tips where special quarter-point elements (QPEs) are utilized. Discretization of the boundary Γ and assembly of equations lead to the transformation of Eq. (1) and (2) into the following matricial form:

$$[Q^1] \{ \theta^F \} = [\Theta^1] \{ q^F \} + \{ B^F \} \quad (3)$$

$$[T] \{ u^F \} = [U] \{ t^F \} + \{ \overline{B}^F \} \quad (4)$$

where F is the current time point and θ^f , q^f are the nodal temperatures and heat fluxes at the time instant $f = 1, F$, respectively. The vectors $\{B^F\}$,

$\{\overline{B}^F\}$ are defined as:

$$\{B^F\} = \sum_{f=1}^{F-1} ([\Theta^{F+1-f}]\{q^f\} - [Q^{F+1-f}]\{\theta^f\}) \quad (5)$$

$$\{\overline{B}^F\} = \sum_{f=1}^F ([\overline{Q}^{F+1-f}]\{\theta^f\} - [\overline{\Theta}^{F+1-f}]\{q^f\}) \quad (6)$$

where $[Q]$, $[\Theta]$, $[T]$, $[U]$, $[\overline{Q}]$, $[\overline{\Theta}]$ are coefficient matrices containing the contributions from Q_i , Θ_i , T_{ij} , U_{ij} , \overline{Q}_i , $\overline{\Theta}_i$, respectively. The vectors $\{\theta\}$, $\{q\}$, $\{u\}$, $\{t\}$ represent nodal boundary values of temperatures, heat fluxes, displacements and tractions, respectively. A constant time interpolation is employed ($\Delta t = t^f - t^{f-1} = \text{const}$) and thus only the matrixes $[Q^1]$ and $[\Theta^1]$ need to be computed and stored in memory for each additional time step [Brebbia, Telles and Wrobel (1984); Raveendra and Banerjee (1992)] during the analysis. The singular diagonal terms of matrixes $[Q^1]$ and $[\Theta^1]$ containing the function $c(\xi)$ and $c_{ij}(\xi)$, respectively, are obtained through the rigid body technique [Brebbia, Telles and Wrobel (1984)].

2.2 Thermal and mechanical contact conditions and assembly of equations

Consider two-dimensional body defined in the domain $\Omega(\Gamma)$, which is bounded by surface Γ . It is assumed that the domain of the problem is divided into sub-domains $^I\Omega$ and $^{II}\Omega$, such that $\Omega(\Gamma) = ^I\Omega(^I\Gamma) + ^{II}\Omega(^{II}\Gamma)$ (see Fig. 1). Part of the boundary of the bodies $^I\Omega$ and $^{II}\Omega$, has the possibility to come into contact and they are defined as master and slave surfaces.

If the boundary surfaces are discretized in elements then a number of master-slave node pairs are created. In the general case, the boundary contact zone consist of three possible contact zones, $\Gamma_o, \Gamma_a, \Gamma_s$, which correspond to the open, adhesion and slip state, denoted as o, a, s , respectively. Additionally, an interface also exists which is characterized by full geometric continuity and compatibility. The Coulomb's law of friction is

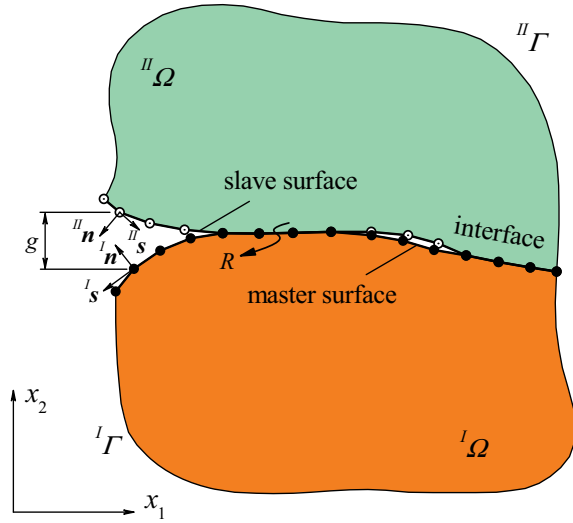


Figure 1: Thermomechanical contact of two elastic bodies

employed to account for frictional contact between the bodies. The mechanical contact conditions are expressed in an average local coordinate system (n, t) , between two nodes of a node-pair, being in one of those contact states (see Fig. 1). Thermal contact conditions are defined according to the assumption that the heat flow between the contacting areas is dependent on the thermal resistance R , which is regarded as a function of contact pressure. The thermal and mechanical contact conditions at a time instant F for a node-pair in adhesion, slip, open state, as well as along the interface are summarized in Tabs. 1 and 2, respectively. In these tables μ represents the coefficient of friction, n, t the local tangential and normal direction and g_n^F expresses the possible initial normal gap between the nodes of a node-pair. If Eqs. (3), (4) are applied to both subregions then the matricial form of equations for the subdomains $I\Omega$ and $II\Omega$ becomes for the thermal part of solution:

$$[{}^I Q^1] \{ {}^I \theta^F \} = [{}^I \Theta^1] \{ {}^I q^F \} + \{ {}^I B^F \} \quad (7)$$

$$[{}^{II} Q^1] \{ {}^{II} \theta^F \} = [{}^{II} \Theta^1] \{ {}^{II} q^F \} + \{ {}^{II} B^F \} \quad (8)$$

and for the mechanical part:

$$[{}^I T] \{ {}^I u^F \} = [{}^I U] \{ {}^I t^F \} + \{ {}^I \bar{B}^F \} \quad (9)$$

$$[{}^{II} T] \{ {}^{II} u^F \} = [{}^{II} U] \{ {}^{II} t^F \} + \{ {}^{II} \bar{B}^F \} \quad (10)$$

Table 1: Thermal conditions

Adhesion – Slip	Open	Interface
${}^I q^F = -{}^{II} q^F$	${}^I q^F = -{}^{II} q^F$	${}^I q^F = -{}^{II} q^F$
${}^I \theta^F = {}^{II} \theta^F - R({}^I t_n^F) {}^I q^F$	${}^I q^F = 0$	${}^I \theta^F = {}^{II} \theta^F$

Table 2: Mechanical conditions

Adhesion	Slip	Open	Interface
${}^I t_t^F = -{}^{II} t_t^F$	${}^I t_t^F = -{}^{II} t_t^F$	${}^I t_t^F = -{}^{II} t_t^F$	${}^I t_t^F = -{}^{II} t_t^F$
${}^I t_n^F = -{}^{II} t_n^F$	${}^I t_n^F = -{}^{II} t_n^F$	${}^I t_n^F = -{}^{II} t_n^F$	${}^I t_n^F = -{}^{II} t_n^F$
${}^I u_t^F = {}^{II} u_t^F$	${}^I t_t^F = \pm \mu {}^I t_n^F$	${}^I t_t^F = 0$	${}^I u_t^F = {}^{II} u_t^F$
${}^I u_n^F = {}^{II} u_n^F - g_n^F$	${}^I u_n^F = {}^{II} u_n^F - g_n^F$	${}^I t_n^F = 0$	${}^I u_n^F = {}^{II} u_n^F$

If the thermal conditions of Tab. 1 are substituted into Eqs. (7)-(8) the resulting equations can be assembled to the following equation referring to the thermal part of the problem:

$$\begin{bmatrix} {}^I Q & 0 & {}^I Q_i & {}^I Q_a & {}^I Q_s & {}^I Q_o & 0 \\ 0 & {}^{II} Q & {}^{II} Q_i & {}^{II} Q_a & {}^{II} Q_s & 0 & {}^{II} Q_o \end{bmatrix} \begin{Bmatrix} {}^I \theta^F \\ {}^{II} \theta^F \\ {}^I \theta_i^F \\ {}^I \theta_\alpha^F \\ {}^I \theta_s^F \\ {}^I \theta_o^F \\ {}^{II} \theta_o^F \end{Bmatrix} = \begin{bmatrix} {}^I \Theta & 0 & {}^I \Theta_i & {}^I \Theta_\alpha & {}^I \Theta_s & {}^I \Theta_o & 0 \\ 0 & {}^{II} \Theta & -{}^{II} \Theta_i & M1 & M2 & 0 & {}^{II} \Theta_o \end{bmatrix} \times \begin{Bmatrix} {}^I q^F \\ {}^{II} q^F \\ {}^I q_i^F \\ {}^I q_\alpha^F \\ {}^I q_s^F \\ {}^I q_o^F \\ {}^{II} q_o^F \end{Bmatrix} + \{ B^F \} \quad (11)$$

where $M1 = -{}^{II} \Theta_\alpha - R({}^I t_{n,\alpha}^F) {}^{II} Q_\alpha$ and $M2 = -{}^{II} \Theta_s - R({}^I t_{n,s}^F) {}^{II} Q_s$.

In the same manner a solvable equation involving the mechanical part of the problem is derived by assembling Eq. (9), (10) according to the mechan-

ical contact conditions provided in Tab. 2 above:

$$\begin{aligned}
 & \begin{bmatrix} {}^I T & 0 & {}^I T_i & {}^I T_a & {}^I T_{t,s} & {}^I T_{n,s} & 0 & {}^I T_o & 0 \\ 0 & {}^{II} T & {}^{II} T_i & {}^{II} T_a & 0 & {}^{II} T_{n,s} & {}^{II} T_{t,s} & 0 & {}^{II} T_o \end{bmatrix} \\
 & \times \begin{pmatrix} {}^I u^F \\ {}^{II} u^F \\ {}^I u_i^F \\ {}^I u_a^F \\ {}^I u_{t,s}^F \\ {}^I u_{n,s}^F \\ {}^{II} u_{t,s}^F \\ {}^I u_o^F \\ {}^{II} u_o^F \end{pmatrix} \\
 & = \begin{bmatrix} {}^I U & 0 & {}^I U_i & {}^I U_a & M3 & {}^I U_o & 0 \\ 0 & {}^{II} U & -{}^{II} U_i & -{}^I U_a & M4 & 0 & {}^{II} U_o \end{bmatrix} \\
 & \times \begin{pmatrix} {}^I t^F \\ {}^{II} t^F \\ {}^I t_i^F \\ {}^I t_a^F \\ {}^I t_{ns}^F \\ -{}^I t_o^F \\ {}^I t_o^F \end{pmatrix} + \{ \overline{B}^F \}
 \end{aligned} \tag{12}$$

where $M3 = {}^I U_{n,s} \pm \mu {}^I U_{t,s}$ and $M4 = -({}^{II} U_{n,s} \pm \mu {}^{II} U_{t,s})$.

In the above equation the subscripts o, a, s , denote the nodes being in open, adhesion and slip state, respectively. Matrices with these subscripts refer to the average local coordinate system in which the corresponding nodes are analyzed (see Fig. 1).

2.3 Iterative procedure for the coupled analysis

It is assumed that the total response time is divided in a number of equal time steps. Each step corresponds to a specific time point t^F which represents the state S^F . The values ${}^I t_{n,a}^F, {}^I t_{n,s}^F$ which express the normal contact pressure along the adhesion and slip areas, are required to evaluate the thermal resistance terms $R({}^I t_{n,a}^F), R({}^I t_{n,s}^F)$ and hence to make Eq. (11) solvable for the state S^F . Due to the fact that ${}^I t_{n,a}^F, {}^I t_{n,s}^F$ are not known and the mechanical part of the problem is not solved yet for the state S^F , it is assumed that $R({}^I t_{n,a}^F) = R({}^I t_{n,a}^{F-1}), R({}^I t_{n,s}^F) = R({}^I t_{n,s}^{F-1})$ where $R({}^I t_{n,a}^{F-1}), R({}^I t_{n,s}^{F-1})$ correspond to the previous

state S^{F-1} and finally Eq. (11) is solved for the state S^{F-1} . Afterwards, the mechanical part of the problem is computed through Eq. (12) considering the contact status of the previous state S^{F-1} . At this stage, every node-pair is examined according to Tab. 3 in order to check if any violations in regard with the geometrical compatibility and traction continuity have occurred. The change in contact or open state is initially checked using the gap g_n^{F-1} of the previous state S^{F-1} . For the node-pair closest to a change, appropriate changes from open to contact state, from adhesion to slip state, and vice versa are made and the new contact condition is applied. Equation (12) is solved again for the state S^F . The node-pairs are checked again (see Tab. 3) and if no changes from contact to open state or vice versa occurs then the new contact status has been evaluated for the state S^F . However, if additional node-pair come to contact or open, additional iterations take place until the imposed constraints of Tab. 3 are satisfied.

Table 3: Definition of contact status

Assumption	Decision	
	Open	Contact
Open	$ {}^{II} u_n^F - {}^I u_n^F > g_n^{F-1}$	$ {}^{II} u_n^F - {}^I u_n^F \leq g_n^{F-1}$
Contact	${}^I t_n^F \geq 0$	${}^I t_n^F < 0$
	Adhesion	
Adhesion	$ {}^I t_i^F < \mu({}^I t_n^F) $	$ {}^I t_i^F \geq \mu({}^I t_n^F) $
Slip	${}^I t_i^F \cdot ({}^I u_i^F - {}^{II} u_i^F) > 0$	${}^I t_i^F \cdot ({}^I u_i^F - {}^{II} u_i^F) \leq 0$

Next, the thermal resistance terms are updated according to the computed tractions ${}^I t_{n,a}^F, {}^I t_{n,s}^F$. Equation (11) is then reconstructed and solved with the new contact status and new thermal resistance terms $R({}^I t_{n,a}^F), R({}^I t_{n,s}^F)$. Having the new thermal solution for the state S^F known, Eq. (12) is resolved and the above-described process continues iteratively. During this iterative procedure, Eqs (11), (12) are solved repeatedly until the contact status does not change and the calculated thermal resistance terms of all adhesion-slip node-pairs of the last iteration R_{last} are approximately equal to the corresponding terms of the previous iteration R_{prev} . If the aforementioned criteria are

fulfilled then the thermal and mechanical solution of state S^F is finalized and the analysis proceeds to the next time point t^{F+1} as far as the computations at the final time point N is completed. This criterion concerning thermal resistance values is expressed as:

$$\left| \frac{R_{last} - R_{prev}}{R_{last}} \right| \times 100 \leq \delta \quad (13)$$

where δ is a small numerical quantity. The last criterion ensures the consistency between thermal and mechanical solutions along the contact zone since the thermal resistance couples the temperature and stress fields. The procedure described above is illustrated in the flow-chart of Fig. 2, where open and contact are denoted as o, c , while the adhesion and slip state when contact occurs are noted as a and s , respectively. It is noted that for the first time point t^0 it is assumed that $R(t_{n,a}^1) = 0$ and $R(t_{n,s}^1) = 0$. Finally, it should be mentioned that the convergence of the numerical solution at any time point is controlled through the typical procedures used in such type of problems and it is improved when more time steps are used and therefore fewer iterations needed until the criteria mentioned above are satisfied.

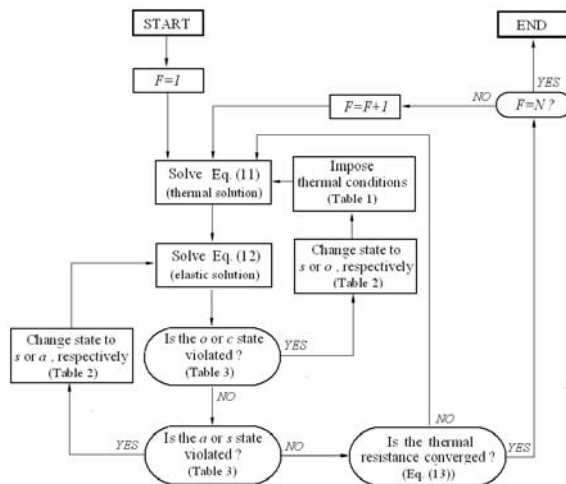


Figure 2: Iterative procedure of the coupled analysis

3 Characterization of interfacial fracture

The present study deals with the computation of fracture characteristics of time-dependent thermally loaded interfacial cracks, existing between dissimilar media. Specifically, these cracks lie in the bond line between two homogeneous isotropic elastic materials. For these bimaterial interface cracks, temperature and heat flux field have an oscillatory behavior near the crack-tip, regardless of the thermal conductivity mismatch [Chen and Huang (1992)]. Thus, as it has been previously mentioned, the well-known quarter-point elements (QPEs) are used for the representation of the near crack tip temperature and displacement field [Martinez and Dominguez (1984); Katsareas and Anifantis (1995)] while traction-singular quarter-point elements (TSQPEs) are utilized to account for the near crack tip heat flux and traction field [Martinez and Dominguez (1984); Katsareas and Anifantis (1995)]. In order to analyze the fracture behavior, the complex stress intensity factor for interfacial cracks in bimetals [Rice and Sih (1965)] defined by the following relationship is introduced:

$$\mathbf{K} = K_I + iK_{II} \quad (14)$$

or equivalently:

$$\mathbf{K} = K_0 e^{i\psi} \quad (15)$$

where $K_0 = \sqrt{K_I^2 + K_{II}^2}$ and $\psi = \tan^{-1}(K_{II}/K_I)$ are the magnitude and the argument of \mathbf{K} , respectively.

The magnitude of K_0 can be calculated by the traction formula [Gao and Tan (1992)] according to the following relationship:

$$K_0 = \frac{\sqrt{2\pi\ell}}{\cosh(\pi\epsilon)} [(t_s^A)^2 + (t_n^A)^2]^{1/2} \quad (16)$$

where s and n refer to the tangential and normal direction, respectively and ℓ is the length of the crack tip element.

Furthermore:

$$\epsilon = 0.5\pi \ln \delta \quad (17)$$

$$\delta = (\mu_1 + \kappa_1 \mu_2) / (\mu_2 + \kappa_2 \mu_1) \quad (18)$$

where μ_d is the shear modulus of the domain $d = 1, 2$ and $\kappa_d = 3 - 4\nu_d$ for plane strain or $\kappa_d = (3 - 4\nu_d)/(1 + \nu_d)$ for plane stress. The superscript A , in Eq. (16) states the node at the crack tip as illustrated in Fig. 3. This formula is very simple since it demands only the calculation of the traction components at the crack tip and it is preferred in the present analysis against the displacement formulas. The accurate evaluation of the crack-tip tractions is achieved using a traction singular quarter point element ahead of the crack tip and fine numerical integration. These tractions are extracted directly by the solution of Eq. (12). Therefore, any computation of stresses on the boundary of the crack through hyper-singular integrals is not necessary.

The fracture characterization of TBC systems, which examined in this study, is made through the calculation of the complex thermal stress intensity factor and the strain energy release rate (SERR) G which is a measure of their fracture resistance efficiency. The SERR is related to the magnitude of complex thermal stress intensity according to the following equation:

$$G = \frac{(K_0)^2}{4} \left(\frac{1 - \nu_C}{\mu_C} + \frac{1 - \nu_S}{\mu_S} \right) \quad (19)$$

4 Numerical results and discussion

At fist the developed formulation is tested through a simple benchmark problem considering imperfect transient thermal contact between two bodies with mismatch in their material properties. The results are compared with data found in the literature and computation by finite elements. Afterwards, the case of a time dependent problem of a thermal barrier coating system with an interfacial central crack is examined. A series of parametric analyses is carried out to account for the crack severity when several scenarios of TCR and combinations of coating and substrate properties are considered. Solutions available in the literature are used for comparisons where possible.

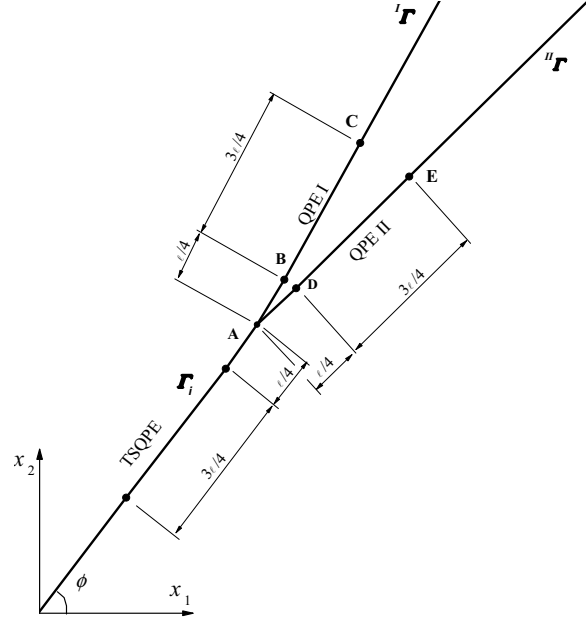


Figure 3: Quarter point elements' configuration at the crack tip

4.1 Transient thermal analysis of two plates with thermal contact resistance

For the two rectangular plates of Fig. 4a plane stress condition is presumed. The length of the plates is $L = 0.1$ m. The aspect L/H is equal to 2. The material properties are as follows: Young's moduli $E^A = E^B = 2.1 \times 10^{11}$ Pa, Poisson's ratios $\nu^A = \nu^B = 0.3$, coefficients of thermal expansion $\alpha^A = 2.25\alpha^B = 22.5 \cdot 10^{-6} \text{ } ^\circ\text{C}^{-1}$ and thermal conductivities $k^A = 1.5 \cdot k^B = 60 \text{ W/m}^2 \text{ } ^\circ\text{C}$. The boundary conditions of the problem are shown in Fig. 4a and the boundary element discretization that was used for the computations is provided in Fig. 4b. It should be noted here that double boundary nodes are placed at the corner points in both thermal and mechanical analyses to account for the discontinuity of tractions and heat fluxes as the outward normal has different direction at each side of the corner. Existence of pressure-dependent TCR is assumed between the contacting surfaces and the cases of TCR-normal traction relations considered are [Kishimoto, Inoue and Shibuya (1995)]:

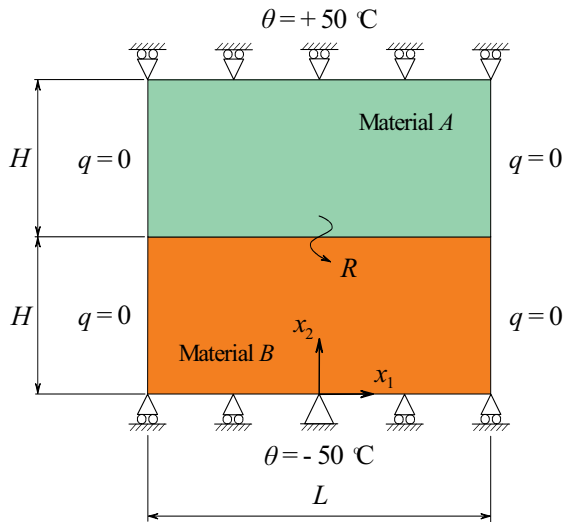
$$R_0 = 0 \quad (20)$$

$$R_1(t_2) = 0.0002 \times \exp(10^{-8}t_2) \quad (21)$$

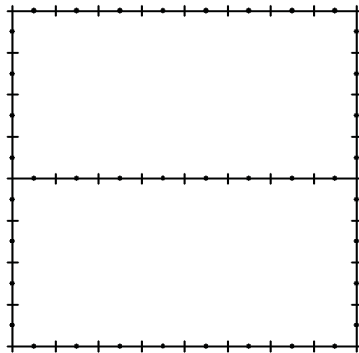
$$R_2(t_2) = 0.002 \times \exp(10^{-8}t_2) \quad (22)$$

$$R_3(t_2) = 0.02 \times \exp(10^{-8}t_2) \quad (23)$$

where t_2 is the normal contact traction in Pa unit. It is noted that Eq. (20) corresponds to perfect thermal contact.



(a) Geometry and boundary conditions



(b) Boundary element mesh

Figure 4: Two rectangular plates in thermomechanical contact

The transient behavior of the system and the evolution of temperature and stress fields are examined. A time period $t_{tot} = 200$ sec is considered and a time step $\Delta t = 2$ sec is utilized. The computations were performed for $\delta = 0.001$ (Eq. (13)).

Figure 5 shows the final temperature distributions along x_2 axis at $x_1 = L/2$ and Fig. 6 illustrates the variation of the final normal contact traction t_2 . Due to the symmetry, only the results for $x_1 \in [0, L/2]$ are demonstrated.

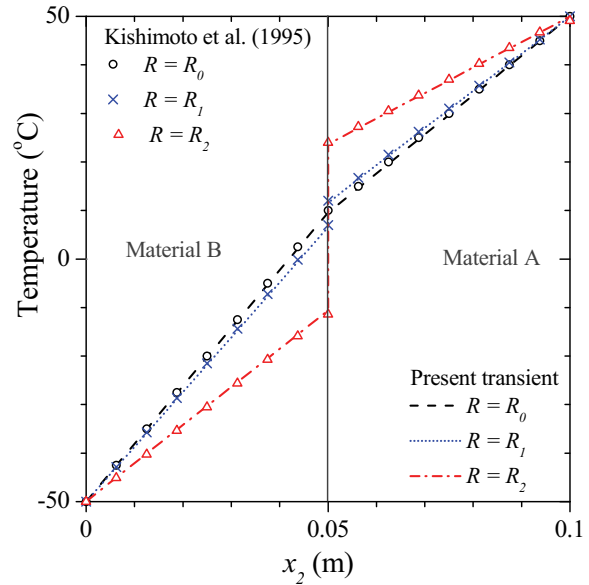


Figure 5: Temperature distribution for different thermal contact resistance scenarios

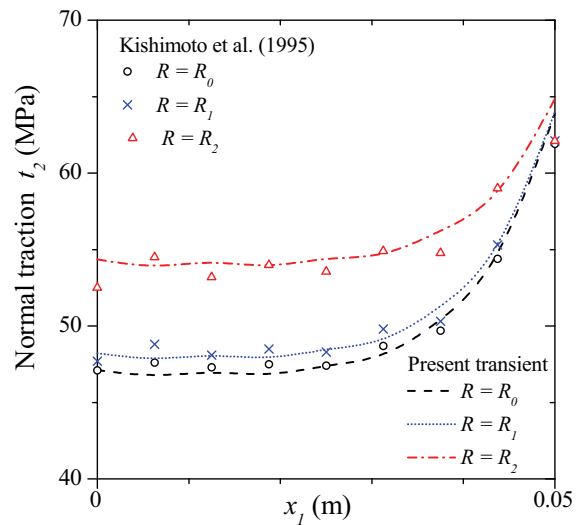


Figure 6: Distribution of normal traction at the interface for different thermal contact resistance scenarios

The results of analyses are depicted in Figs. 5, 6

for temperature and normal traction, respectively and are plotted against those given by Kishimoto, Inoue and Shibuya (1995) which refer to the steady state of this problem. Apparently, the large time period of 200 sec, which has been considered in the present transient analysis, it is enough to derive the steady state solution. In Fig. 5, the temperature distribution along the thickness of the bimaterial solid exhibits a jump at the interface because of the existence of TCR. The higher the TCR is, the higher the jump in temperature since the heat conduction between the surfaces is restricted. In Fig. 6, the normal traction along the interface is presented for three levels of TCR. The analysis showed that higher values of thermal resistance lead to the increase of normal contact stress while the pick value appears at the edge of the contacting faces. Obviously, results of the present coupled analysis compares well with the steady state solution of Kishimoto, Inoue and Shibuya (1995).

The temperature and stress distributions along the same cross sections as presented in Figs. 5-6, at several time points are illustrated in the series of Figs. 7a-7b and 8a-8b, respectively.

Specifically, Figs. 7a-7b depict the temperatures at 20, 40 and 200 seconds assuming TCR R_1 and R_2 , respectively (Eqs. (21), (22) and Figs. 8a, b provide the normal traction t_2 for the above cases. In all graphs results of the present boundary element analysis are compared to results of finite element analyses conducted by the authors due to the lack of transient analysis with pressure-dependent TCR in the literature. The finite element results were obtained using the commercial package ANSYS. According to Figs. 7a-7b the distribution of temperature is not-linear during the first seconds of the heat exchange and gradually it tends to the linear profile which represents the steady state. The jump in temperature is increased as the heat exchange is evolved.

On the contrary, Figs. 8a-8b show a similar distribution of the normal traction at any time instant for both levels of TCR. The contact pressure is increased with time taking its maximum values at the steady state. In all cases the results of finite and boundary element analyses compare fa-

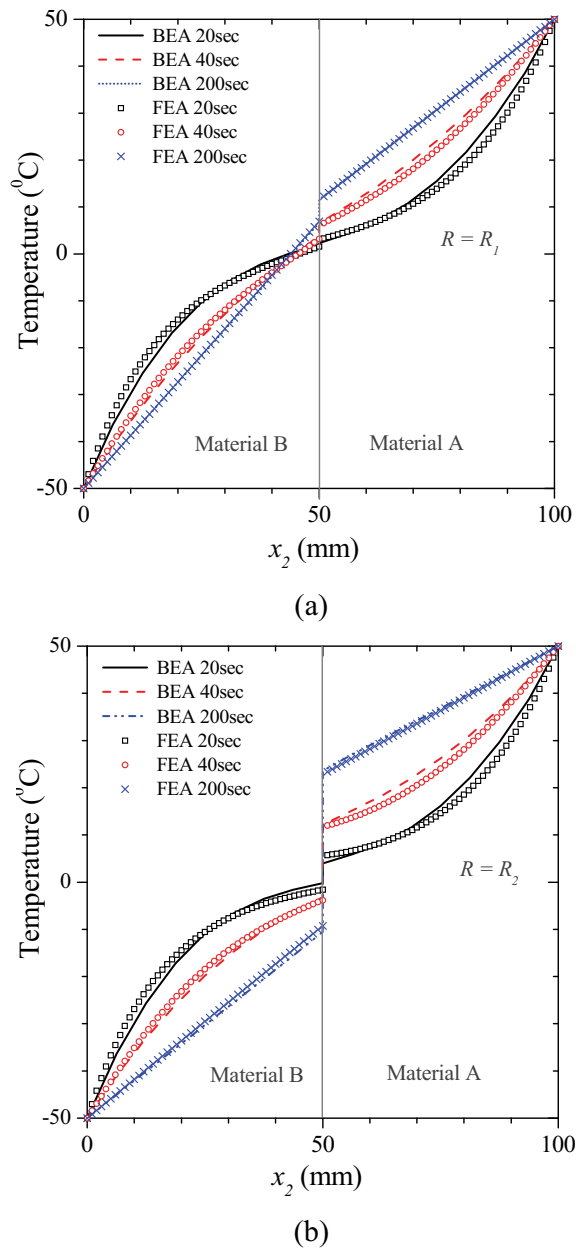
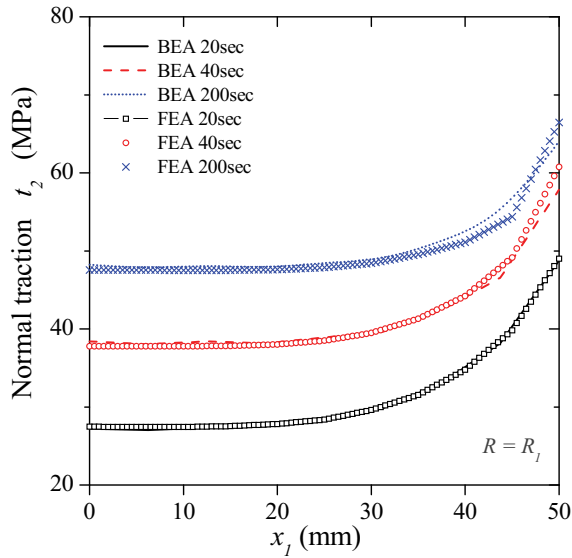


Figure 7: Comparison between temperature distributions computed by FEA and BEA at different time points for TCR: (a) $R = R_1$ and (b) $R = R_2$

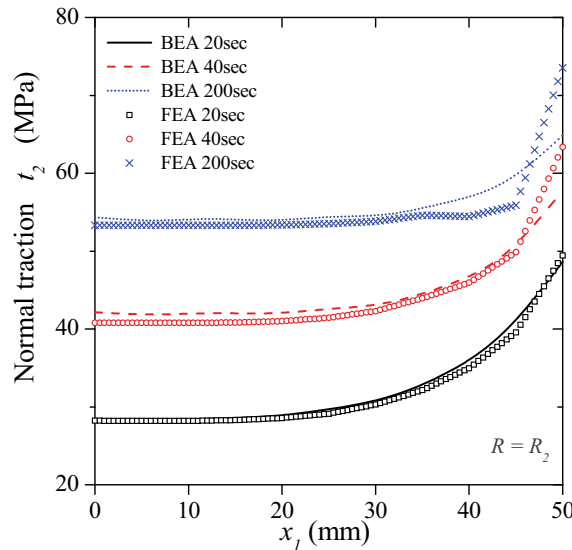
vorably encouraging the present formulation.

4.2 Thermal shock of a TBC system with an interfacial central crack

The developed boundary element formulation is adopted in order to study the transient fracture problem of the TBC system shown in Fig. 9a.



(a)

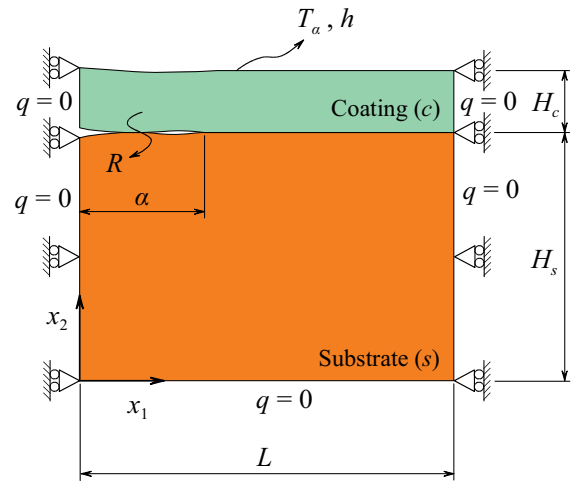


(b)

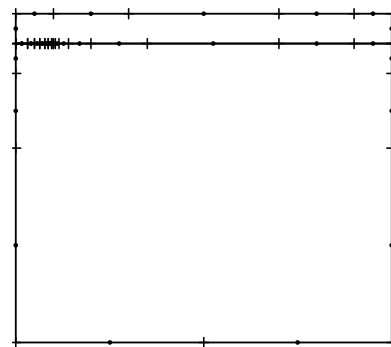
Figure 8: Comparison between normal traction distributions along the interface computed by FEA and BEA at different time points for TCR: (a) $R = R_1$ and (b) $R = R_2$

Due to the symmetry only the half of the system modeled. The problem consists of two subdomains, a coating layer of thickness H_c and a substrate of thickness $H_s = 10H_c$. An interfacial central crack of length $2a = 2(H_s/8)$ exists between the two layers. Fig. 9a shows the boundary conditions and geometrical aspects of the BEM model

and the mesh is given in Fig. 9b. Similarly to the problem examined in 4.1, double boundary nodes are used at any corner point as well as at the crack tip.



(a) Geometry and boundary conditions



(b) Boundary element mesh

Figure 9: Model of a TBC system with an interfacial central crack

After tests it was proved that a length $L = 10a$ is more than sufficient for the time-dependent solution to converge to the solution of the infinite problem (for $L > 10a$ the vertical constraints on the right would not have any effect on the solution). The material that is used as coating is Zirconia (ZrO_2), while nodular cast iron is used as substrate. In essence, it is a simple ceramic-to-metal bond and not an integrated TBC system, since

the metallic bond coat, which is applied between the ceramic top coat and the substrate, [Rangaraj and Kokini (2003); Arai, Okajima and Kishimoto (2007)] is not considered here, for reasons of simplicity. The material properties are provided in Tab. 4. The TBC system has an initial temperature T_0 and experiences a thermal shock as the free surface of the coating is heated by the ambient temperature $T_\alpha \gg T_0$ considering a coefficient of heat convection $h_0=50 \text{ W/m}^2 \text{ }^\circ\text{C}$. Plane strain conditions are assumed.

Table 4: Material properties of the thermal barrier coating system

Property	Zirconia (coating)	Nodular cast iron (substrate)
Young Modulus (GPa)	200	168
Poisson's ratio	0.23	0.31
Coefficient of thermal expansion ($^\circ\text{C}^{-1}$) $\times 10^{-6}$	10.2	13.7
Thermal conductivity ($\text{W/m}^\circ\text{C}$)	2.2	48.9
Density (kg/m^3)	5900	7290
Specific heat ($\text{J/kg }^\circ\text{C}$)	460.6	418.4

This transient problem has been examined by Kokini and Reynolds (1991) using finite elements. In that work, the problem was solved for a finite length of $L=32a$ assuming frictionless and adiabatic contact. Since it was proved in the present work that for $L > 10a$ the same transient behavior of G^* is obtained, a comparison between the two studies for the case $\mu = 0$ and $R = \infty$ can be made. In order to achieve convergent time behaviors of G^* , quarter point elements of lengths $\ell = a/20$ were selected. Constant time steps $\Delta t^*=0.00162$ for $0.00162 \leq t^* \leq 0.0324$ and $\Delta t^*=0.0162$ for $0.0324 \leq t^* \leq 0.324$ were utilized, since it was proved that they were sufficient to produce convergent solution. In order to reduce the computational effort, crack faces were discretized into 7 + 7 elements while both bodies were divided into 23 (substrate) + 22 (coating) elements. This coarse mesh was selected after a mesh convergence test which showed that finer meshes for the discretiza-

tion of the crack surfaces produce the same time behaviors of G^* . The heating of the upper surface of the coating results to the creation of compressive tractions which finally lead to crack closure. This adhesive or sliding contact is taken into account in order to determine the temperature field around the crack lips. The lack of appropriate data from the literature for the relation of thermal resistance with the contact pressure for material used in TBC systems leads to the consideration of function of Eqs. (20)-(23) for imperfect thermal contact [Kishimoto, Inoue and Shibuya (1995)]. This full or partial conductance may have significant impact on the produced displacement and stress field. The results are presented in terms of the following non-dimensional parameters:

$$G^* = \frac{G}{E_C \alpha_C^2 (\Delta T)^2 H_S}, \quad t^* = \frac{k_C t}{\rho_C c_C H_S^2} \quad (24)$$

The evolution of non-dimensional SERR G^* is presented in Fig. 10 for perfect, imperfect and adiabatic contact (insulation) conditions. The case considered here represents frictionless contact ($\mu = 0$). If insulation between the crack faces is assumed the current results can be directly compared to finite element results of Kokini and Reynolds (1991).

The comparison reveals remarkable agreement between the present methodology and FE results. Apparently, the existence of pressure TCR has a significant influence on the developed G^* . The extreme cases of thermal insulation and perfect thermal contact between the crack faces delimit the values of G^* and the higher the TCR the higher the stress intensity leading to the upper bound of G^* when adiabatic contact ($R = \infty$) is assumed. The differences in G^* values between these two cases is about of an order of magnitude. Low TCR values reduce the jump in temperature at the interface and the stress distribution derives lower strain energy release rates. The analyses give very similar results when R_0 (Eq. (20)) or R_1 (Eq. (21)) is considered for the TCR-normal traction relation and in essence R_1 corresponds to perfect thermal contact. Additionally, the time points at which the peak values of G^* is independent from the level of TCR. Obviously, disregarding the partial conductance between the crack faces in contact the

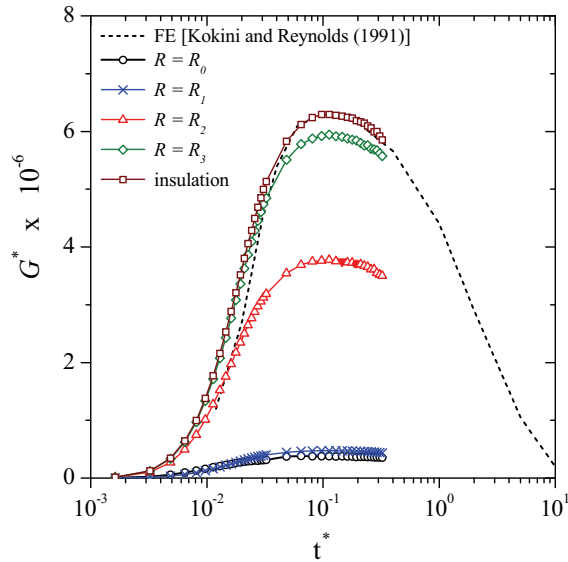


Figure 10: Non-dimensional G^* versus non-dimensional time for several levels of thermal contact resistance

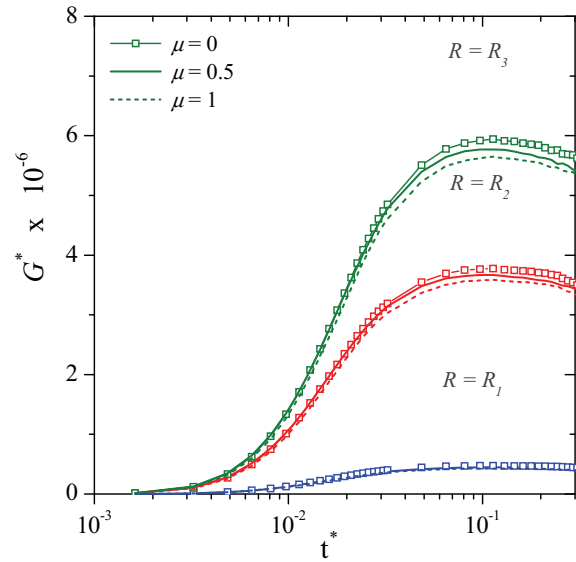


Figure 11: Non-dimensional G^* versus non-dimensional time for various combinations of thermal contact resistance and coefficient of friction

fracture assessment of TBC systems lead to conservative estimation of their fracture resistance.

In Fig. 11, G^* is plotted against the time for several combinations of coefficient of friction and TCR. The friction coefficient has not a remarkable influence on G^* because the normal contact stresses has relatively low values resulting to low tangential frictional stresses (Coulomb's law). Therefore, for reasons of computational simplicity all the subsequent analyses consider frictionless contact and results refer to the case of $\mu = 0$.

The peak values of G^* are very sensitive to the magnitude of the heat transfer coefficient h . Thus, apart from the original case $h_0=50 \text{ W/m}^2\text{°C}$ the problem was solved for additional heat transfer coefficients. The results are summarized in Fig. 12 which show the variation of peak values of SERR, G^*_{peak} , with respect to the ratio h/h_0 , respectively. As it can be seen from Fig. 12 G^*_{peak} is rapidly increased for greater ratios h/h_0 especially for higher values of TCR, exhibiting a linear behavior in this double logarithmic scale. This diagram is an indication that assuming high TCR or thermal insulation, the crack severity may be overestimated for very intense thermal shocks.

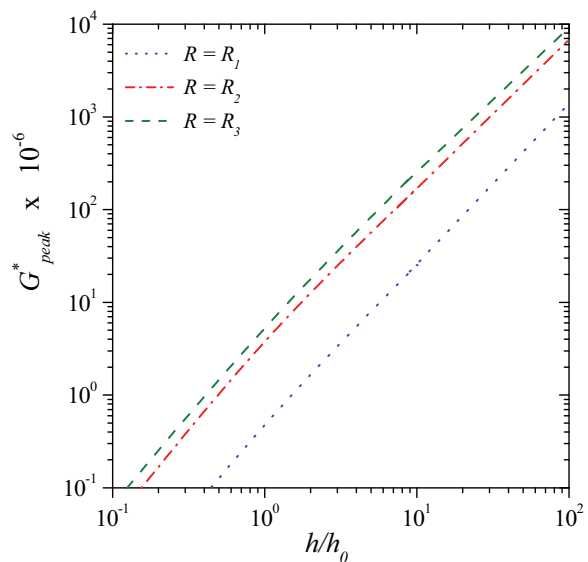


Figure 12: Peak values of the non-dimensional SERR versus heat transfer coefficient ratio h/h_0 for different thermal contact resistance functions

The mechanical and thermal properties of a TBC can be customized if it is composed of a number of layers, each one being a mixture of ceramics and metal alloy of several volume fractions [Rangaraj and Kokini (2003)]. Such combina-

tions lead to a functionally graded TBC with properties different of those of the original ceramic coating. The following parametric study was conducted for ratios of thermal expansion coefficients $\alpha^* = \alpha_c/\alpha_s$ and thermal conductivities $k^* = k_c/k_s$ where the indices c, s , denote the coating and substrate respectively.

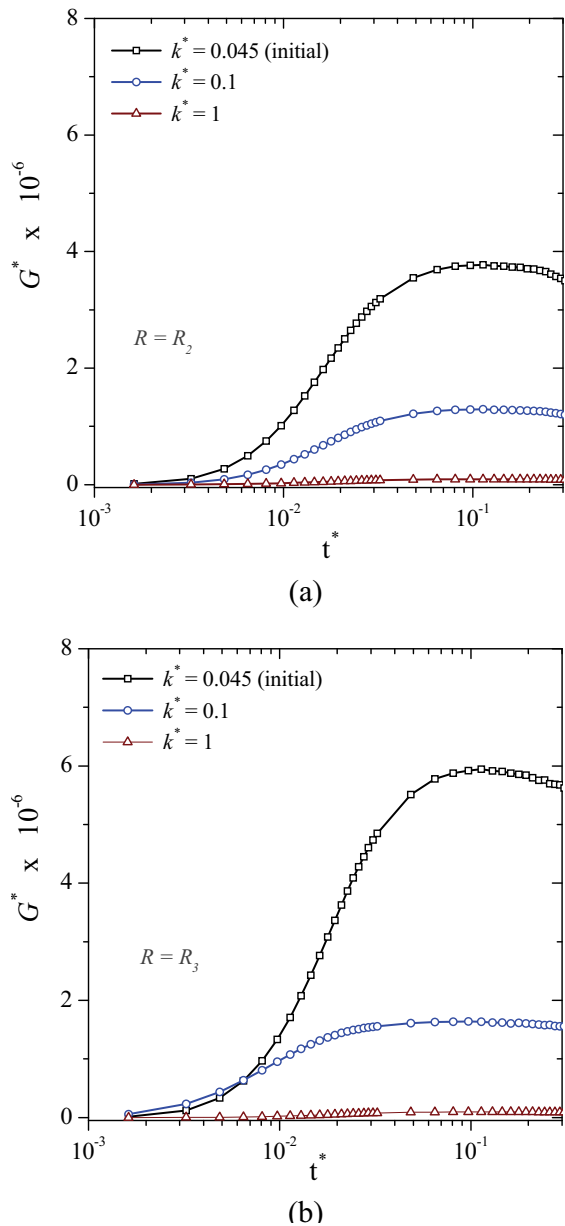


Figure 13: Effect of thermal conductivities ratio on transient G^* for TCR: (a) $R = R_2$ and (b) $R = R_3$

Figures 13a-b depict the transient G^* , for various k^* , when R_2 or R_3 (Eq. (22)-(23)) is considered. The graphs show that the higher k^* the lower the SERR. This dependency is well pronounced for both R_2 and R_3 and of course the higher TCR R_3 (Fig. 13b), yields higher G^* values. A low conductivity of the coating does not permit rapid spread of the heat over the thickness of TBC when the coating surface withstands a thermal shock. Consequently, the temperature jump on either side of the interface is high producing great SERR. On the other hand the lower the mismatch in thermal expansion coefficient α^* the lower the developed SERR. This is evident in Figs. 14a-b for R_2 or R_3 , respectively where the evolution of G^* with time is presented for several values of α^* .

Obviously, the effect of α^* is more significant. When increasing α^* one order of magnitude, G^* is increased two orders of magnitude. It is noticeable that the transient behavior of the crack is similar for every combination of TCR or material incompatibility since the peak value of the non-dimensional G^* appears almost at the same time t^* .

All cases examined above are summarized in Fig. 15 for thermal conductivity mismatch and Fig. 16 for thermal expansion mismatch in respect with the peak value of SERR, G_{peak}^* since the time behavior is similar for any case.

These two graphs afford valuable information to the designer of a TBC system. The failure resistance of such system can be improved when the thermal conductivities ratio k^* is increased (see Fig. 15) and the ratio of coefficients of thermal expansion ratio α^* is decreased (see Fig. 16) disregarding the level of TCR between the contacting crack faces. Additionally, for any material combination the fracture assessment is highly sensitive to the level of pressure-dependent TCR that is incorporated in analysis. The results show that the difference in G_{peak}^* when the extreme cases of thermal insulation and perfect thermal contact are adopted is about one order of magnitude. Certainly, both hypotheses are not valid and an intermediate level of resistance is representative for this problem with partial crack face contact. Therefore, considering adiabatic contact the crack

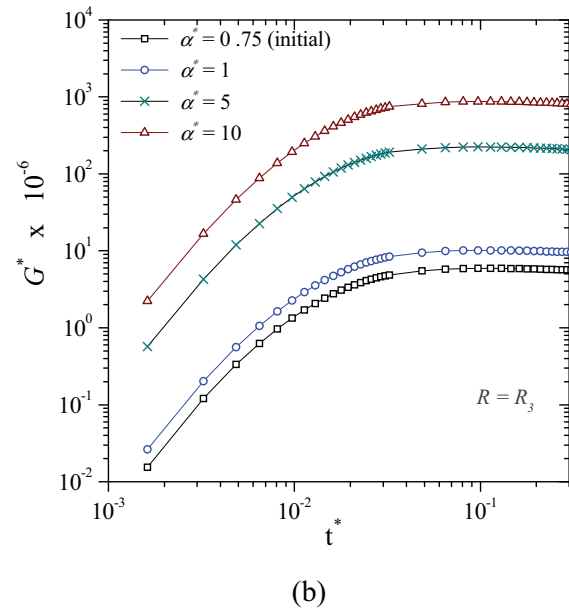
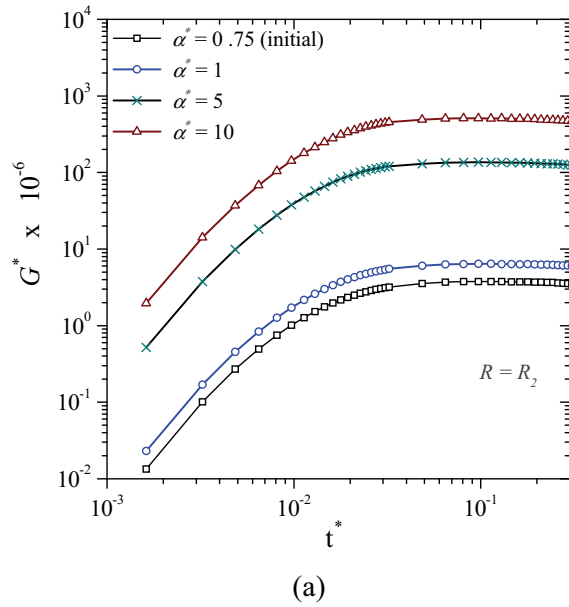


Figure 14: Effect of thermal conductivities ratio on transient G^* for TCR: (a) $R = R_2$ and (b) $R = R_3$

severity may be overestimated giving a conservative evaluation of the failure resistance.

5 Conclusions

A boundary element formulation capable of treating time-dependent, coupled thermoelastic contact problems, where pressure-dependent thermal

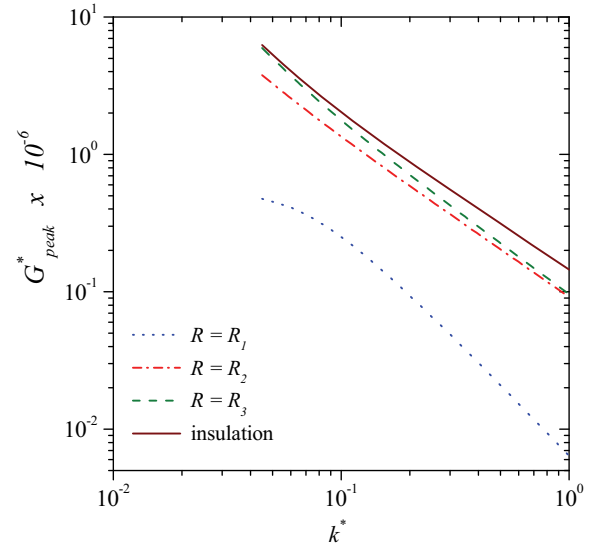


Figure 15: Sensitivity of the peak values of the non-dimensional SERR to the combination of thermal conductivities ratio with the level of TCR

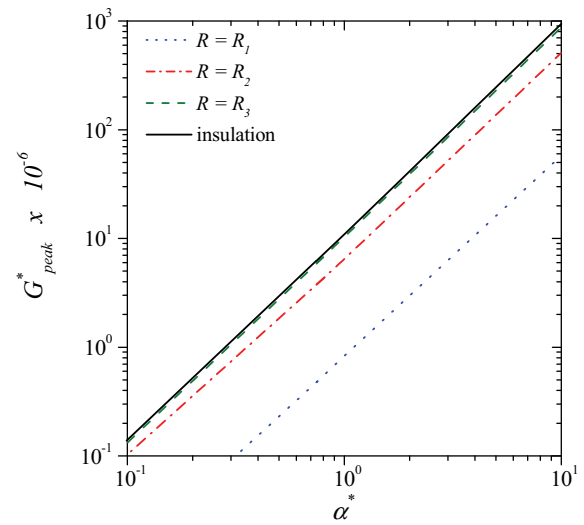


Figure 16: Sensitivity of the peak values of the non-dimensional SERR to the combination of the thermal expansion coefficients ratio with the level of TCR

resistance between contacting faces is involved, was presented. The approach is based on sub-regional technique and iterative procedure between time-increments. The time-evolution of temperature within the thickness or at the interface of two solids in contact can be easily computed. In an effort to emphasize the impact of

thermal contact resistance on the fracture assessment the proposed methodology has been applied to a thermal barrier coating system under thermal shock when a stationary interface crack is present. The consideration of different levels of thermal contact resistance between the crack faces, especially when the heat flow is perpendicular to the crack, may lead to conservative or optimistic conclusions about the fracture resistance of the system utilizing as index the strain energy release rate. The higher the thermal contact resistance is, the higher the severity of the crack especially under very high heating rates. Furthermore in the framework of parametric analysis it was found that the presence of coefficient of friction has a little effect on the strain energy release rate. Also, the lower the thermal conductivity of the coating is, the higher the value of the strain energy release rate. On the contrary lower values of thermal expansion coefficient of the coating reduce the SERR. Apparently, it can be concluded that the effect of pressure-dependent thermal resistance may be considerable in cases of fracture assessment of bimaterial solids under thermal shock and appropriate boundary elements formulations can be very efficient for the solution of this class of problems.

References

- Alonso, M. P.; Garrido, J.A.** (1995): BEM applied to 2D thermoelastic contact problems including conduction and forced convection in interstitial zones. *Engineering Analysis with Boundary Elements*, vol. 15 pp. 249-259.
- Alonso, M. P.; Garrido, J.A.; Foces, A.** (1995): Application of BEM to solve two-dimensional thermoelastic contact problems with convection and radiation conditions. *Computers & Structures* vol. 66, pp. 115-125.
- Arai, M.; Okajima, Y.; Kishimoto, K.** (2007): Mixed-mode interfacial fracture toughness for thermal barrier coating. *Engineering Fracture Mechanics*, vol. 74, pp. 2055-2069.
- Barber, J.R.; Comninou, M.** (1983): The penny-shaped interface crack with heat flow: 2. Imperfect contact. *Journal of Applied Mechanics*, vol. 50, pp. 770-776.
- Blandford, G.E.; Tauchert, T.R.** (1985): Thermoelastic analysis of layered structures with imperfect layer contact. *Computers & Structures*, vol. 21, pp. 1283-1291.
- Brebbia, C.A.; Telles J.C.; Wrobel, L.C.** (1984): *Boundary Element Techniques*, Springer, Berlin.
- Chen, W.H.; Huang, C.C.** (1992): On the singularity of temperature gradient near an inclined crack terminating at bimaterial interface. *International Journal of Fracture*, vol. 58, pp. 319-324.
- Chen, X.; Liu, Y.** (2001): Thermal Stress Analysis of Multi-layer Thin Films and Coatings by an Advanced Boundary Element Method. *CMES: Computer Modelling in Engineering & Sciences*, vol.2, pp. 337-349.
- Ching, H. K.; Chen, J. K.** (2006): Thermomechanical Analysis of Functionally Graded Composites under Laser Heating by the MLPG Method. *CMES: Computer Modelling in Engineering & Sciences*, vol.13, pp.199-217.
- Comninou, M.; Barber, J.R.** (1984): The thermoelastic Hertz problem with pressure dependent contact resistance. *International Journal of Mechanical Sciences*, vol. 26, pp. 549-554.
- Gao, Y.L.; Tan, C.L.** (1992): Determination of characterizing parameters for bimaterial interface cracks using the boundary element method. *Engineering Fracture Mechanics*, vol. 41, pp. 779-784.
- Giannopoulos, G.I.; Anifantis, N.K.** (2007): A BEM analysis for thermomechanical closure of interfacial cracks incorporating friction and thermal resistance. *Computer Methods in Applied Mechanics and Engineering*, vol. 196, pp. 1018-1029.
- Hattiangadi, A.; Siegmund, T.** (2005): A numerical study on interface crack growth under heat flux loading. *International Journal of Solids and Structures*, vol 42, pp. 6335-6355.
- Katsareas, D.E.; Anifantis, N.K.** (1995): Performance of quarter-point boundary elements in analyzing thermally stressed and curved cracks. *Computer Methods in Applied Mechanics and En-*

gineering, vol. 137, pp. 153-165.

Kishimoto, K.; Inoue, H.; Shibuya, T. (1995): A boundary element analysis of thermoelastic contact problems. *Engineering Analysis with Boundary Elements*, vol. 15, pp.329-337.

Kokini K.; Reynolds, R.R. (1991): Transient heating vs cooling of interfacial cracks in ceramic-to-metal bonds. *Engineering Fracture Mechanics*, vol. 38, pp. 371-383.

Kuo, A.Y. (1990): Effects of crack surface heat conductance on stress intensity factors. *Journal of Applied Mechanics*, vol. 57, pp. 354-358.

Martinez, J.; Dominguez, J. (1984): On the use of quarter-point boundary elements for stress intensity factor computations. *International Journal for Numerical Methods in Engineering*, vol. 20, pp. 1941-1950.

Martynyak, R.M.; Honchar, Kh.I.; Nahalka, S.P. (2003): Simulation of thermomechanical closure of an initially open interface crack with heat resistance. *Materials Science*, vol. 39, pp. 672-681.

Pantuso, D.; Bathe, K.J.; Bouzinov, P.A. (2000): A finite element procedure for analysis of thermo-mechanical solids in contact. *Computers and Structures*, vol. 75, pp. 551-573.

Rangaraj, S.; Kokini, K. (2003): Interface thermal fracture in functionally graded zirconia-mullite-bond coat alloy thermal barrier coatings. *Acta Materialia*, vol. 51, pp. 251-267.

Raveendra, S.T.; Banerjee, R.K. (1992): Boundary element analysis of cracks in thermally stressed planar structures. *International journal of Solid and Structures*, vol. 29, pp. 2301-2317.

Rice, J.R.; Sih, G.C. (1965): Plane problems of cracks in dissimilar media. *Journal of Applied Mechanics*, vol. 32, pp. 418-423.

Rizk Abd El-Fattah, A. (1993): A cracked plate under transient thermal stresses due to surface heating. *Engineering Fracture Mechanics*, vol. 45, pp. 687-696.

Shiah, Y.C.; Tan, C.L. (2000): Fracture Mechanics Analysis in 2-D Anisotropic Thermoelasticity Using BEM. *CMES: Computer Modelling in Engineering & Sciences*, vol. 1, pp. 91-99.

Shiah, Y.C.; Guao, T.L.; Tan, C.L. (2005): Two-Dimensional BEM Thermoelastic Analysis of Anisotropic Media with Concentrated Heat Sources. *CMES: Computer Modelling in Engineering & Sciences*, vol.7, pp.321-338.

Sih, G.C.; Chen, C.K. (1986): Growth of a crack caused by temperature gradients with change in surface insulation. *Theoretical and Applied Fracture Mechanics*, vol. 5, pp. 101-107.

Sladek, J.; Sladek, V.; Zhang, Ch.; Tan, C.L. (2006): Meshless Local Petrov-Galerkin Method for Linear Coupled Thermoelastic Analysis. *CMES: Computer Modelling in Engineering & Sciences*, vol.16, pp.57-68.

Zavarise, G.; Wriggers, P.; Stein, E.; Schrefler, B.A. (1992): Real contact mechanisms and finite element formulation – a coupled thermomechanical approach. *International Journal for Numerical Methods in Engineering*, vol. 35, pp. 767-785.